

# Domain Adaptation As a Problem of Inference on Graphical Models

Kun Zhang<sup>1\*</sup>   Mingming Gong<sup>2\*</sup>   Petar Stojanov<sup>1</sup>   Biwei Huang<sup>1</sup>  
Clark Glymour<sup>1</sup>

<sup>1</sup>Carnegie Mellon University, Pittsburgh, PA 15213, USA

<sup>2</sup>University of Melbourne, Melbourne, VIC, Australia

## Abstract

This paper is concerned with data-driven unsupervised domain adaptation, where it is unknown in advance how the joint distribution changes across domains, i.e., what factors or modules of the data distribution remain invariant or change across domains. To develop an automated way of domain adaptation with multiple source domains, we propose to use a graphical model as a compact way to encode the change property of the joint distribution, which can be learned from data, and then view domain adaptation as a problem of Bayesian inference on the graphical models. Such a graphical model distinguishes between constant and varied modules of the distribution and specifies the properties of the changes across domains, which serves as prior knowledge of the changing modules for the purpose of deriving the posterior of the target variable  $Y$  in the target domain. This provides an end-to-end framework of domain adaptation, in which additional knowledge about how the joint distribution changes, if available, can be directly incorporated to improve the graphical representation. We discuss how causality-based domain adaptation can be put under this umbrella. Experimental results on both synthetic and real data demonstrate the efficacy of the proposed framework for domain adaptation.

## 1 Introduction

Over the past decade, various approaches to unsupervised domain adaptation (DA) have been pursued to leverage the source-domain data to make prediction in the new, target domain. In particular, we consider the situation with  $n$  source domains in which both the  $d$ -dimensional feature vector  $X$ , whose  $j$ th dimension is denoted by  $X_j$ , and label  $Y$  are given, i.e., we are given  $(\mathbf{x}^{(i)}, \mathbf{y}^{(i)}) = (\mathbf{x}_k^{(i)}, y_k^{(i)})_{k=1}^{m_i}$ , where  $i = 1, \dots, n$ , and  $m_i$  is the sample size of the  $i$ th source domain. We denote by  $x_{jk}^{(i)}$  the value of the  $j$ th feature of the  $k$ th data point (example) in the  $i$ th domain. Our goal is to find the classifier for the target domain, in which only the features  $\mathbf{x}^T = (\mathbf{x}_k^T)_{k=1}^m$  are available. Because the distribution may change across domains, clearly the optimal way of adaptation or transfer depends on what information is shared across domains and how to do the transfer.

In the covariate shift scenario, the distribution of the features,  $P(X)$ , changes, while the conditional distribution  $P(Y|X)$  remains fixed. A common strategy is to reweight examples from the source domain to match the feature distribution in the target domain—an approach extensively studied in machine learning; see e.g., [1, 2, 3, 4, 5, 6]. A common prerequisite for such an approach is that the support for the source domain include the target domain, but of course this is often not the case.

---

\*equal contribution

Another collection of methods learns a domain-invariant feature representation that has identical distributions across the target and source domains [7, 8, 9, 10, 11].

In addition, it has been found that  $P(Y|X)$  usually changes across domains, in contrast to the covariate shift setting. For the purpose of explaining and modeling the change in  $P(Y|X)$ , the problem was studied from a generative perspective [12, 13, 14, 15, 16]—one can make use of the factorization of the joint distribution corresponding to the causal representation and exploit how the factors of the joint distribution change, according to commonsense or domain knowledge. The settings of target shift [12, 16, 14, 17, 18] and conditional shift [14, 19, 20] assume only  $P(Y)$  and  $P(X|Y)$  change, respectively, and their combination, as generalized target shift [14, 21], was also studied, and the corresponding methods clearly improved the performance on a number of benchmark datasets. The methods were extended further, by learning feature representations with invariant conditionals given the label and matching joint distributions [19, 22, 23], and it was shown how methods based on domain-invariant representations can be understood from this perspective.

How are the distributions in different domains related? Essentially, DA aims to discover and exploit the constraints in the data distribution implied by multiple domains and make prediction that adapts to the target domain. To this end, we assume that the distributions of the data in different domains were independent and identically distributed (I.I.D.) drawn from some “mother” distribution. The mother distribution encodes the uncertainty in the domain-specific distributions, i.e., how the joint distribution is different across the domains. Suppose the mother distribution is known, from which the target-domain distribution is drawn. Furthermore, the target domain contains data points (without  $Y$  values) generated by this distribution. It is then natural to leverage both the mother distribution and the target-domain feature values to reveal the property of the target-domain distribution for the purpose of predicting  $Y$ . In other words, DA is achieved by exploiting the mother distribution and the target-domain feature values to derive the information of  $Y$ .

Following this argument, we have several questions to answer. First, is there a natural, compact description of the constraints on the changes of the data distribution (to describe the mother distribution)? Such constraints include which factors of the joint distributions can change, whether they change independently, and the range of changes. (We represent the joint distribution as a product of the factors.) Second, how can we find such a description from the available data? Third, how can we make use of such a description as well as the target-domain data to make optimal prediction? Traditional graphical models have provided a compact way to encode conditional independence relations between variables and factorize the joint distribution [24, 25]. We will use an extension of Directed Acyclic Graphs (DAGs), called augmented DAGs, to factorize the joint distribution and encode which factors of the joint distribution change across domains. The augmented DAG, together with the conditional distributions and changeability of the changing modules, gives a augmented graphical model as a compact representation of how the joint distribution changes. Predicting the  $Y$  values in the target domain is then a problem of Bayesian inference on this graphical model given the observed target-domain feature values. This provides a natural framework to address the problem of DA in an automated, end-to-end manner.

## 2 DA and Inference on Graphical Models

For the purpose of discover what to transfer in a automated way, in this paper we *mainly consider DA with at least two source domains*, although the method can be applied to the single-source case if proper additional constraints are known. Generally speaking, the availability of multiple source domains provides more hints helpful to find  $P^T(X|Y)$  as well as  $P^T(Y|X)$ . Several algorithms have been proposed to combine source hypothesis from multiple source domains in different ways [26, 27, 28, 29]. As one may see, existing methods mainly assume the properties of the distribution shift and utilize the assumptions for DA; furthermore, the involved assumptions are usually rather strong. Violation of the assumptions may lead to negative transfer.

An essential question then naturally arises—is it possible to develop a data-driven approach to automatically figure out what information to transfer from the sources to the target and make optimal prediction in the target domain, under mild conditions? This paper aims at an attempt to answer this question, by representing the properties of distribution change with a graphical model, estimating the graphical model from data, and treating prediction in the target domain as a problem of inference on the graphical model given the target-domain feature values. Below we present the used graphical models and how to use them for DA.

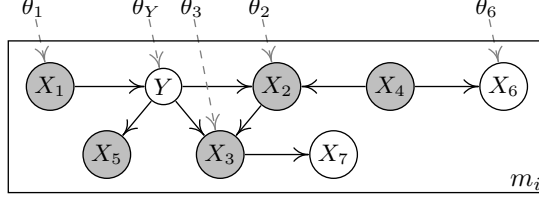


Figure 1: An augmented DAG over  $Y$  and  $X_i$ . See main text for its interpretation.

## 2.1 Describing Distribution Change Properties with Augmented Graphical Models

In the target domain, the  $Y$  values are to be predicted, and we aim at their optimal prediction with respect to the joint distribution. To find the target-domain distribution, one has to leverage source-domain data and exploit the connection between the distributions in different domains. It is then natural to factorize the joint distribution into different components or modules—it would facilitate recovering the target distribution if as few components as possible change across the domains. Furthermore, in estimation of the changing modules in the target domain, it will be beneficial if those changes are not coupled so that one can do “divide-and-conquer”; otherwise, if the changes are coupled, one has to estimate the changes together and would suffer from “curse-of-dimensionality.” In other words, DA benefits from a compact description of how the data distribution can change across domains—such a description, together with the given feature values in the target domain, helps recover the target joint distribution and enables optimal prediction. In this section we introduce our graphical model as such a way to describe distribution changes.

Traditional graphical models provide a compact, yet flexible, way to decompose the joint distribution of as a product of simpler, lower-dimensional factors [30, 25], as a consequence of conditional independence relations between the variables. For our purpose, we need encode not only conditional independence relations between the variables, but also whether the conditional distributions change across domains. To this end, we propose an augmented Directed Acyclic Graph (DAG) as a flexible yet compact way to describe how a joint distribution changes across domains, assuming that the distributions in all domains can be represented by such a graph. It is an augmented graph in the sense that it is over not only features  $X_i$  and  $Y$ , but also external latent variables  $\theta$ .

Figure 1 gives an example of such a graph. Nodes in gray are in the Markov Blanket (MB) of  $Y$ . The  $\theta$  variables are mutually independent, and take the same value across all data points within each domain and may take different values across domains. They indicate the property of distribution shift—for any variable with a  $\theta$  variable directly into it, its conditional distribution given its parents (implied by the DAG over  $X_i$  and  $Y$ ) depends on the corresponding  $\theta$  variable, and hence may change across domains. In other words, the distributions across domains differ only in the values of the  $\theta$  variables. Once their values are given, the domain-specific joint distribution is given by  $P(\mathbf{X}, Y | \theta)$ , which can be factorized according to the augmented DAG. In the example given in Figure 1, distribution factors  $P(X_1)$ ,  $P(Y|X_1)$ , and  $P(X_3|Y, X_2)$ , among others, change across domains, while  $P(X_5|Y)$  and  $P(X_7|X_3)$  are invariant. The joint data distribution in the  $i$ th domain can be written as

$$P(\mathbf{X}, Y | \theta^{(i)}) = P(X_1 | \theta_1^{(i)}) P(Y | X_1, \theta_Y^{(i)}) P(X_5 | Y) P(X_2 | Y, X_4, \theta_2^{(i)}) P(X_3 | Y, X_2, \theta_3^{(i)}) \times \\ P(X_4) P(X_6 | X_4, \theta_6^{(i)}) P(X_7 | X_3).$$

We have several remarks to make on the used augmented graph. First, since the  $\theta_i$  are independent, the corresponding conditional distributions change independently across domains. Because of such a independence property, one can model and learn the changes in the corresponding factors separately. Second, we note that each node in the augmented graph may be a set of variables, as a “supernode” instead of a single one. For instance, for the digit recognition problem, one can view the pixels of the digit image as such a “supernode” in the graph.

### 2.1.1 Relation to Causal Graphs

If the causal graph underlying the observed data is known, there is no confounder (hidden direct common cause of two variables), and the observed data are perfect random samples from the populations, then one can directly benefit from the causal model for transfer learning, if it is known,

as shown in [31, 14, 32]. In fact, in this case our graphical representation will encode the same conditional independence relations as the original causal model.

It is worth noting that the causal model, on its own, might not be sufficient to explain the properties of the data, for instance, because of selection bias [33], which is often present in the sample. Furthermore, it is notoriously difficult to find causal relations based on observational data; to achieve it, one often has to make rather strong assumptions on the causal model (such as faithfulness [34]) and sampling process. On the other hand, it is rather easy to find the graphical model purely as a description of conditional independence relationships in the variables as well as the properties of changes in the distribution modules. The underlying causal structure may be very different from the augmented DAG we adopt. For instance, let  $Y$  be disease and  $X$  the corresponding symptoms. It is natural to have  $Y$  as a cause of  $X$ . Suppose we have data collected in different clinics (domains) and that subjects are assigned to different clinics in a probabilistic way according to how severe the symptoms ( $X$ ) are. Then one can see that across domains we have changing  $P(X)$  but a fixed  $P(Y|X)$  and, accordingly, in the augmented DAG has a directed link from  $X$  to  $Y$ , contrary to the causal direction. For detailed examples as well as the involved causal graphs and augmented DAGs, please see Appendix A1.

## 2.2 Inference on Augmented Graphical Models for DA

We now aim to predict the value of  $Y$  given the observed features  $\mathbf{x}^\tau$  in the target domain, which is about  $P(\mathbf{Y}^\tau | \mathbf{x}^\tau)$ , where  $\mathbf{Y}^\tau$  is the concatenation of  $Y$  across all data points in the target domain. To this end, we have several issues to address. First, which features should be included in the prediction procedure? Second, as illustrated in Figure 1, a number of distribution factors change across domains, indicated by the links from the  $\theta$  variables, and it is not necessary to consider all of them for the purpose of DA—which changing factors should be adapted to the target-domain data?

Let us first show the general results on calculation of  $P(\mathbf{Y}^\tau | \mathbf{x}^\tau)$ , based on which prediction in the target domain is made. We then discuss how to simplify the estimator, thanks to the specific augmented graphical structure over  $\mathbf{X}$  and  $Y$ . As the data are I.I.D. given the values of  $\theta$ , we know  $P(\mathbf{x}, \mathbf{y} | \theta) = \prod_k P(\mathbf{x}_k, y_k | \theta)$  and  $P(\mathbf{x} | \theta) = \prod_k P(\mathbf{x}_k | \theta)$ . Also bearing in mind that the value of  $\theta$  is shared within the same domain, we have

$$P(\mathbf{Y}^\tau = \mathbf{y}^\tau | \mathbf{x}^\tau) = \int P(\mathbf{y}^\tau | \mathbf{x}^\tau, \theta) P(\theta | \mathbf{x}^\tau) d\theta \quad (1)$$

where  $P(\theta | \mathbf{x}^\tau) = \prod_k [\sum_{y_k^\tau} P(\mathbf{x}_k^\tau, y_k^\tau | \theta)] P(\theta) / \int \prod_k [\sum_{y_k^\tau} P(\mathbf{x}_k^\tau, y_k^\tau | \theta)] P(\theta) d\theta$ . For computational efficiency, we make prediction separately for different data points based on

$$P(y_k^\tau | \mathbf{x}^\tau) = \sum_{y_{k'}^\tau, k' \neq k} P(\mathbf{y}^\tau | \mathbf{x}^\tau) = \int P(y_k^\tau | \mathbf{x}_k^\tau, \theta) P(\theta | \mathbf{x}^\tau) d\theta. \quad (2)$$

In the above expression,  $P(\theta)$  is given in the augmented graphical model,  $P(y_k^\tau, \mathbf{x}_k^\tau | \theta)$  can be calculated by using the chain rule on the augmented graphical model. Here we assume that the density  $P(y_k^\tau, \mathbf{x}_k^\tau | \theta)$  is tractable, and we will show approximate inference procedures in Section 3.3 when we use implicit models to model  $P(\mathbf{x}_k^\tau, y_k^\tau | \theta)$ . Also,  $P(y_k^\tau | \mathbf{x}_k^\tau, \theta)$  can be estimated by training a probabilistic classifier on the generated data from our model.

Moreover, for the purpose of predicting  $Y$ , not all  $X_j$  are needed for the prediction of  $Y$ , and not all changing distribution modules need to adapt to the target domain. We exploit the graph structure to simplify the above expression. Let  $\mathbf{V} = \mathbb{CH}(Y) \cup \{Y\}$ , where  $\mathbb{CH}(Y)$  denotes the set of children of  $Y$  relative to the considered augmented DAG. Also denote by  $\mathbb{PA}(V_j)$  the parent set of  $V_j$ . The conditional distribution of  $V_j$  given its parents is  $P(V_j | \mathbb{PA}(V_j), \theta_{V_j})$ , where  $\theta_{V_j}$  is the empty set if this conditional distribution does not change across domains. Let

$$\mathcal{C}_{jk} := P(v_{jk}^\tau | \mathbb{PA}(v_{jk}^\tau), \theta_{V_j}) \quad (3)$$

be shorthand for the conditional distribution of  $V_j$  taking value  $v_{jk}^\tau$  conditioning on its parents taking the  $k$ th value in the target domain and the value of  $\theta_{V_j}$ .  $P(\mathbf{x}_k^\tau, y_k^\tau | \theta)$  can be factorized as

$$P(\mathbf{x}_k^\tau, y_k^\tau | \theta) = \left[ \prod_{V_j \in \mathbf{V}} \mathcal{C}_{jk} \right] \cdot \underbrace{\left[ \prod_{W_j \notin \mathbf{V}} P(w_{jk}^\tau | \mathbb{PA}(w_{jk}^\tau), \theta_{W_j}) \right]}_{\triangleq N_k, \text{ which does not depend on } y_k^\tau}.$$

Substituting the above expression into Eq. 2, one can see that  $N_k$ , defined above, will not appear in the final expression, so finally

$$P(y_k^\tau | \mathbf{x}^\tau) = \int P(y_k^\tau | \mathbf{x}_k^\tau, \boldsymbol{\theta}) \frac{\prod_k [\sum_{y_k^\tau} \prod_{V_j \in \mathbf{V}} C_{jk}] \prod_{V_j \in \mathbf{V}} P(\theta_{V_j})}{\int \prod_k [\sum_{y_k^\tau} \prod_{V_j \in \mathbf{V}} C_{jk}] \prod_{V_j \in \mathbf{V}} P(\theta_{V_j}) d\boldsymbol{\theta}} d\boldsymbol{\theta}. \quad (4)$$

It is natural to see from the above final expression of  $P(y_k^\tau | \mathbf{x}^\tau)$  that 1) only the conditional distributions for  $Y$  and its children (variables in  $\mathbf{V}$ ) need to be adapted (their corresponding  $\boldsymbol{\theta}$  variables are involved in the expression) and that 2) among all features, only those in the MB of  $Y$  are involved in the expression.

### 2.2.1 Benefits from a Bayesian Treatment

Many traditional procedures for unsupervised DA are concerned with the identifiability of the joint distribution in the unlabeled target domain [31, 14, 35]. If the joint distribution is identifiable, a classifier can be learned by minimizing the loss with respect to the target-domain joint distribution. For instance, the so-called location-scale transformation is assumed for the features given the label  $Y$  [14], rendering the target-domain joint distribution identifiable. Otherwise, successful DA is not guaranteed without further constraints. Even in the situation where the target-domain joint distribution is not identifiable, the Bayesian treatment, by incorporating the prior distribution of  $\boldsymbol{\theta}$  and inferring the posterior of  $Y$  in the target domain, may provide very informative prediction—the prior distribution of  $\boldsymbol{\theta}$  constrains the changeability of the distribution modules, and such constraints may enable “soft” identifiability. For an illustrative example on this, please see Appendix A2.

## 3 Implementation of Data-Driven DA

In practice we are given data and the graphical model is often not available. For DA, we then need to learn (the relevant part of) the augmented graphical model from data, which includes the augmented DAG structure, the conditional distribution of each variable in  $\mathbb{CH}(Y) \cup \{Y\}$  given its parents, and the prior distribution of the relevant  $\boldsymbol{\theta}$  variables, and then develop computational methods for inferring  $Y$  on it given the target-domain data.

### 3.1 Learning the Augmented DAG

For wide applicability of the proposed method, we aim to find a nonparametric method to learn the augmented DAG, instead of assuming restrictive conditional models such as linear ones. We note that in the causality community, finding causal relations from nonstationary or heterogeneous data has attracted some attention in recent years. In particular, under a set of assumptions, a nonparametric method to tackle this causal discovery problem, called Causal Discovery from Nonstationary/heterogeneous Data (CD-NOD) [36, 37], was recently proposed. The method is an extension of the PC algorithm [38] and consists of 1) figuring out where the causal mechanisms change, 2) estimation of the skeleton of the causal graph, and 3) determination of more causal directions compared to PC by using the independent change property of causal modules. Here we adapt their method for learning the portion of the augmented DAG needed for DA, without resorting to the assumptions made in their work.

Denote by  $\mathbf{S}$  the set of  $Y$  and all  $X_i$ . The adapted method has the following three steps. The first two are directly adapted from CD-NOD. *Step 1* is to Find changing distribution factors and estimate undirected graph. Let  $C$  be the domain index. It applies the first stage of the PC algorithm to  $\mathbf{S} \cup \{C\}$  to find an undirected graph. It is interesting to note that if variable  $S_i \in \mathbf{S}$  is adjacent to  $C$ , then  $S_i$  is conditionally dependent on  $C$  given *any* subset of the remaining variables, and hence,  $P(S_i | \mathbb{PA}(S_i))$  must change across domains. *Step 2* is to determine edge directions, by applying the orientation rules in PC, with the additional constraints that all the  $\boldsymbol{\theta}$  variables are exogenous and independent. Furthermore, if  $S_i$  and  $S_j$  are adjacent and are both adjacent to  $C$ , use the direction between them which gives independent changes in their conditional distributions,  $P(S_i | \mathbb{PA}(S_i))$  and  $P(S_j | \mathbb{PA}(S_j))$  [37]. If the changes are dependent in both directions, merge  $S_i$  and  $S_j$  as (part of) a “supernode”, and merge their corresponding  $\boldsymbol{\theta}$  variables. *Step 3* finally Instantiates a DAG from the output of Step 2, which is a partially DAG. For details of this procedure, see Appendix A3.

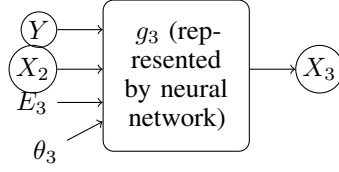


Figure 2: LV-CGAN for modeling  $P(X_3 | Y, X_2, \theta_3)$  implied by the graph given in Figure 1.

### 3.2 Latent-Variable CGAN for Modeling Changing Conditional Distributions

The second practical issue to be addressed is how to represent and learn the conditional distributions involved in (4). In light of the power of the Generative Adversarial Network (GAN) [39] in capturing the property of high-dimensional distributions and generating new random samples and the capacity of Conditional GAN (CGAN) [40] in learning flexible conditional distribution, we propose an extension of CGAN, namely, Latent-Variable CGAN (LV-CGAN), to model and learn a class of conditional distributions  $P(S_i | \mathbb{P}\mathbb{A}(S_i), \theta_{S_i})$ , with  $\theta_{S_i}$  as a latent variable. As an example, Figure 2 shows the structure of the LV-CGAN to model the conditional distribution of  $P(X_3 | Y, X_2)$  across domains implied by the augmented DAG given in Figure 1. The whole network, including its parameters, is shared, and only the value of  $\theta_3$  may vary across domains. Hence, it explicitly models both changing and invariant portions in the conditional distribution. In the  $i$ -th domain,  $\theta_3$  takes value  $\theta_3^{(i)}$  and encodes the domain-specific information. The network specifies a model distribution  $Q(X_3 | Y, X_2, \theta_3)$  by the generative process  $X_3 = g_3(Y, X_2, E_3, \theta_3)$ , which transforms random noise  $E_3$  to  $X_3$ , conditioning on  $Y$ ,  $X_2$ , and  $\theta_3$ .  $E_3$  is independent of  $Y$  and  $X_2$ , and its distribution is fixed (we used the standard Gaussian distribution).  $g_3$  is a function represented by a neural network (NN) and shared by all domains.  $Q(X_3 | Y, X_2, \theta_3^{(i)})$  is trained to approximate the conditional distribution  $P(X_3 | Y, X_2)$  in the  $i$ th domain. For invariant conditional distributions such as  $P(X_5 | Y)$  in Figure 1, the  $\theta$  input vanishes and it becomes a CGAN.

### 3.3 Learning and Inference

Because we use GAN to model the distributions, the inference rules (2) and (4) are not be directly applied because of the intractability of the involved distributions. To tackle this problem, we develop a stochastic variational inference (SVI) [41] procedure to directly approximate the posterior  $P(\theta | \mathbf{x}^\tau, \mathbf{y}^\tau)$  in the source domain and  $P(\theta | \mathbf{x}^\tau)$  in the target domain. For simplicity of notation, we denote the  $i$ -th source domain data as  $\mathcal{D}^i$ , the target domain data as  $\mathcal{D}^\tau$ , and the combined source and target domain data as  $\mathcal{D}$ . We rely on the evidence lower bound (ELBO) of marginal likelihood in both source and target domains:

$$\begin{aligned} \log p(\mathcal{D}) \geq & - \sum_{i=1}^s \text{KL}(q(\theta | \mathcal{D}^i) | p(\theta)) + \mathbb{E}_{q(\theta | \mathcal{D}^i)} \left[ \sum_{k=1}^{m_i} \log p_g(\mathbf{x}_k^{(i)}, y_k^{(i)} | \theta) \right] \\ & - \text{KL}(q(\theta | \mathcal{D}^\tau) | p(\theta)) + \mathbb{E}_{q(\theta | \mathcal{D}^\tau)} \left[ \sum_{k=1}^m \log p_g(\mathbf{x}_k^\tau | \theta) \right]. \end{aligned} \quad (5)$$

We approximate the posterior of  $\theta$  in source and target domains with the Gaussian distribution  $q(\theta | \mathcal{D}^i) = \mathcal{N}(\theta | \mu^{(i)}, \sigma^{(i)})$ ,  $q(\theta | \mathcal{D}^\tau) = \mathcal{N}(\theta | \mu^\tau, \sigma^\tau)$ . Then we can learn the model parameters in  $g$  as well as the variational parameters in each domain by the variational EM algorithm.

Up to now, we have followed the standard SVI procedure and assume that the density  $p_g(X, Y, \theta)$  induced by the GAN generator  $g$  is tractable, which is not true in our case. To extend the standard SVI for implicit distributions, we replace  $\sum_{k=1}^{m_i} \log p_g(\mathbf{x}_k^{(i)}, y_k^{(i)} | \theta)$  with Jensen-Shannon divergence or Maximum Mean Discrepancy [42] that compares the empirical distributions of the  $i$ -th source domain data and the data generated from  $g$ . We perform the same procedure in the target domain. More details and theoretical justification of this procedure can be found in Appendix A4.

After learning the variational parameters, we can sample  $\theta$  for the target domain and generate samples from  $g$  to learn a classifier that approximate the posterior  $P(y_k^\tau | \mathbf{x}^\tau)$ . To make the procedure more efficient, we can make use of the decomposition of the joint distribution  $p_g(X, Y | \theta)$  over the augmented graph, as shown in Eq. 4. The detailed derivations and justifications can be found in Appendix A5.

Table 1: Accuracy on simulated datasets for the baselines and proposed method. The values presented are averages over 10 replicates for each experiment. Standard deviation is in parentheses.

	DICA	weigh	simple_adapt	comb_classif	LMP	poolSVM	Infer
9 sources	80.04(15.5)	72.1(14.5)	70.0(14.3)	72.34(16.24)	78.90(13.81)	71.8(11.43)	<b>83.90(9.02)</b>
4 sources	74.16(13.2)	67.88(13.7)	65.22(16.00)	69.64(15.8)	79.06(13.93)	70.08(12.25)	<b>85.38(11.31)</b>
2 sources	86.56(13.63)	75.04(18.8)	69.42(17.87)	74.28(18.2)	84.52(13.72)	83.84(13.7)	<b>93.10(7.17)</b>

## 4 Experiments

### 4.1 Simulations

We simulate binary classification data from the graph on Figure 1, where we vary the number of source domains between 2, 4 and 9. We model each module in the graph with 1-hidden-layer MLPs with 32 nodes. In each replication, we randomly sample the MLP parameters and domain-specific  $\theta$  values from  $N(0, \mathbf{I})$ . We sampled 500 points in each source domain and the target domain. We compare our approach, denoted by *Infer* against alternatives. We include a hypothesis combination method, denoted *simple\_adapt* [26], linear mixture of source conditionals [15] denoted by *weigh* and *comb\_classif* respectively. We also compare to the pooling SVM (denoted *poolSVM*), which merges all source data to train the SVM, as well as domain-invariant component analysis (DICA) [43], and Learning marginal predictors (LMP) [44]. The results are presented in Table 1. From the results, it can be seen that the proposed method outperforms the baselines by a large margin. Regarding significance of the results, we compared our method with the two other most powerful methods (DICA and LMP) using Wilcoxon signed rank test. The the p-values are 0.074, 0.009, 0.203 (against DICA) and 0.067, 0.074, 0.074 (against LMP), for 2, 4, and 9 source domains, respectively.

### 4.2 Wi-Fi Localization Dataset

We then perform evaluations on the cross-domain indoor WiFi location dataset [45]. The WiFi data were collected from a building hallway area, which was discretized into a space of grids. At each grid point, the strength of WiFi signals received from  $D$  access points was collected. We aim to predict the location of the device from the  $D$ -dimensional WiFi signals.

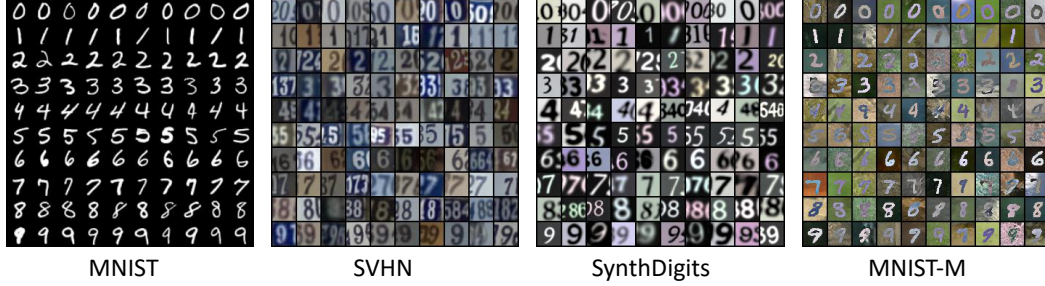
For the multiple-source setting, we cast it as a classification problem, where each location is assigned with a discrete label. We consider the task of transfer between different time periods, because the distribution of signal strength changes with time while the underlying graphical model is rather stable, which satisfies our assumption. The WiFi data were collected by the same device during three different time periods  $t_1$ ,  $t_2$ , and  $t_3$  in the same hallway. Three sub-tasks including  $t_2, t_3 \rightarrow t_1$ ,  $t_1, t_3 \rightarrow t_2$ , and  $t_1, t_2 \rightarrow t_3$  are taken for performance evaluation. We thus obtained 19 possible labels, and in each domain we sampled 700 points in 10 replicates. We learn the graphical model and changing modules from the two source domains, and perform learning and Bayesian inference in all the domains. The graph learned from the Wifi  $t_1$  and  $t_2$  data is given in the Appendix A6. We implement our LV-CGAN by using Multi-Layer Perceptions (MLPs) with one hidden layer (32 nodes) to model the function of each module and set the dimension of input noise  $E$  and  $\theta$  involved in each module to 1. The reported result is classification accuracy of location labels. We use the same baselines as in the simulated dataset, excluding *simple\_adapt* and *comb\_classif*, and add a stronger baseline *poolNN* which replaces SVM in *poolSVM* with NN. We also compare with a recent adversarial learning method *Soft-Max* [46]. We present the results in Table 2. The results show that our method outperforms all baselines by a large margin.

### 4.3 Flow Cytometry Dataset

We also evaluate our method on the Graft vs. Host Disease Flow Cytometry dataset (GvHD) [47]. The dataset consists of blood cells from patients, and the task is to classify each cell whether it is a lymphocyte based on cell surface biomarkers. It is reasonable to assume that each patient has a different distribution of cells, and being able to predict the cell type in a new unlabeled patient given existing labeled patient data is an important task. There are 29 patients with 7 cell surface biomarkers, and we performed 29 experiments for each patient, where we treat it as a target domain subsample rest of the patients as source domains. We use the same baseline methods as in the Wifi dataset. We present classification accuracy results for 3 and 5 source domains in Table 2. The results show that

Table 2: Accuracy on the Wi-Fi &amp; Flow data. Standard deviation is in parentheses.

	DICA	weigh	LMP	poolSVM	Soft-Max	poolNN	Infer
t2, t3 $\rightarrow$ t1	29.32(2.5)	43.71(3.02)	46.80(1.4)	40.25(1.6)	44.86(5.1)	42.88(1.6)	<b>64.22(5.2)</b>
t1, t3 $\rightarrow$ t2	24.5(3.6)	38.19(1.9)	39.11(2.1)	48.70(1.8)	44.95(4.4)	47.41(2.1)	<b>66.75(6.0)</b>
t1, t2 $\rightarrow$ t3	21.7(3.9)	36.03(1.85)	39.28(2.05)	40.46(1.4)	43.63(4.1)	41.00(1.8)	<b>74.05(2.7)</b>
Flow 3 sources	79.2(11.0)	84.2(9.3)	91.6(8.4)	92.1(7.5)	89.0(9.7)	95.7(5.2)	<b>96.6(2.1)</b>
Flow 5 sources	83.1(12.0)	92.9(7.0)	92.3(6.4)	94.7(6.1)	89.7(8.0)	96.0(5.1)	<b>97.9(2.2)</b>

Figure 3: The generated images in each domain in the T+S+D/M task. Each row of an image corresponds to a fixed  $Y$  value, ranging from 0 to 9. MNIST-M is the unlabeled target domain and the rest are source domains.

our method is much better than most of the methods and performs slightly better than poolNN, which is a very strong baseline on this dataset.

#### 4.4 Digits Datasets

Following the experimental setting in [46], we build a multi-source domain dataset by combining four digits datasets, including MNIST, MNIST-M, SVHN, and SynthDigits. We take MNIST, MNIST-M, and SVHN in turn as the target domain and use the rest domains as source domains, which leads to three domain adaptation tasks. We randomly sample 20,000 labeled images for training in the source domain, and test on 9,000 examples in the target domain. We use  $Y \rightarrow X$  (as in previous work such as [35]), where  $X$  is the image, as the graph for adaptation. We leverage a recently proposed twin auxiliary classifier GAN framework [48] to match conditional distributions of generated and real data. More implementation details can be found in the Appendix A7.

We compare our method with recent deep multi-source adaptation method MDAN [46], with two variants Hard-Max and Soft-Max, and several baseline methods evaluated in [46], including poolNN and denoted *weight* described above and poolDANN) that considers the combined source domains as a single source domain and perform the DANN method [11]. Because our classifier network is different from that used in [46], we also report the poolNN method with our network architecture, denoted as poolNN\_Ours.

The quantitative results are shown in Table 3. It can be seen that our method achieves much better performance than alternatives on the two hard tasks. This is very impressive because our baseline classifier (poolNN\_Ours) performs worse poolNN in [46]. Figure 3 shows the generated images in each domain in the T+S+D/M task. Each row of an image corresponds to a fixed  $Y$  value, ranging from 0 to 9. It can be seen that our method generates correct images for the corresponding labels, indicating that our method successfully transfer label knowledge from source domains and recovers the conditional distribution  $P_{X|Y}$  (also  $P_{Y|X}$ ) in the unlabeled target domain. The generated images for the other two tasks are given in the Appendix A8.

Table 3: Accuracy on the digits data. T: MNIST; M: MNIST-M; S: SVHN; D: SynthDigits.

	weigh	poolNN	poolDANN	Hard-Max	Soft-Max	poolNN_Ours	Infer
$S + M + D/T$	75.5	93.8	92.5	97.6	<b>97.9</b>	94.9	96.64
$T + S + D/M$	56.3	56.1	65.1	66.3	68.7	59.6	<b>89.89</b>
$M + T + D/S$	60.4	77.1	77.6	80.2	81.6	67.8	<b>89.34</b>



## 5 Conclusion and Discussions

In this paper, we proposed a framework to deal with unsupervised domain adaptation with multiple source domains by considering domain adaptation as an inference problem on a particular type of graphical model over the target variable and features or their combinations as super-nodes, which encodes the change properties of the data across domains. The graphical model can be directly estimated from data, leading to an automated, end-to-end approach to domain adaptation. As future work, we will study how the sparsity level of the learned graph affects the final prediction performance and, more importantly, aim to improve the computational efficiency of the method by resorting to more efficient inference procedures. Dealing with transfer learning with different feature spaces (known as heterogeneous transfer learning) by extending our approach is also a direction to explore.

# Appendices

## A1. Examples to Illustrate the Difference between Causal Graph and Our Augmented DAG

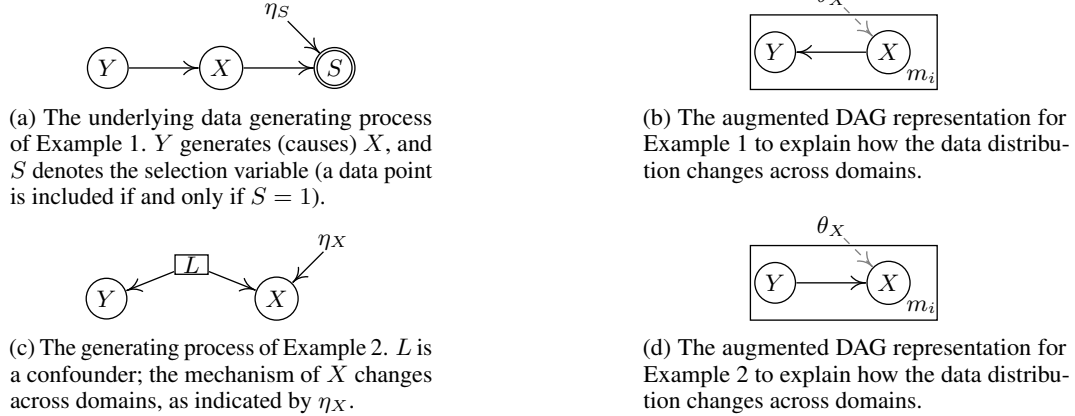


Figure 4: Two examples to illustrate the difference between the underlying causal graph and the augmented DAG used to represent the property of distribution changes across domains. (a) and (c) are the causal graphs of the two examples, and (b) and (d) the corresponding augmented DAGs.

Here we give two simple examples to illustrate the possible difference between the underlying causal structure and the graph we use for domain adaption. In Example 1, let  $Y$  be disease and  $X$  the corresponding symptoms. It is natural to have  $Y$  as a cause of  $X$ . Suppose we have data collected in different clinics, each of which corresponds to a domain. Further assume that subjects are assigned to different clinics in a probabilistic way according to how severe the symptoms are. Figure 4(a) gives the causal structure together with the sampling process to generate the data in each domain.  $S$  is a selection variable, and a data point is selected if and only if  $S$  takes value 1.  $P(S = 1|X)$  depends on  $\eta_S$ , which may take different values across domains, reflecting different sampling mechanisms (e.g., subjects go to different clinics according to their symptoms). In this case, according to data in different domains,  $P(X)$  changes. But  $P(Y|X)$  will stay the same because according to the process given in (a),  $Y$  and  $S$  are conditionally independent given  $X$  and, as a consequence,  $P(Y|X, S) = P(Y|X)$ . The graphical model for describing the distribution change across domains is given in 4(b)—they are apparently inconsistent, and the direction between  $Y$  and  $X$  is reversed; however, for the purpose of DA, the graph in (b) suffices and, furthermore, as shown later, it can be directly learned from data from multiple domains. Example 2 follows the causal structure given in Figure 4(c), where  $X$  and  $Y$  are not directly causally related but have a hidden direct common cause (confounder)  $L$  and the generating process of  $X$  also depends on  $\eta_X$ , whose value may vary across domains. We care only about how the distribution changes—since in this example  $P(Y)$  remains the same across domains, we can factorize the joint distribution as  $P(Y, X) = P(Y)P(X|Y)$ , in which only  $P(X|Y)$  changes across domains, and the corresponding augmented DAG is shown in (d).

## A2. Illustration of Benefits from a Bayesian Treatment

Here is an example showing the benefits of a Bayesian treatment. For clarity purposes, we use simple parametric models and a single feature  $X$  for the conditional distributions:  $Y \sim \mathcal{N}(0, \theta_Y)$ ,  $X = Y + E$ , where  $E \sim \mathcal{N}(0, \theta_X)$ , i.e.,  $X|Y \sim \mathcal{N}(Y, \theta_2)$ . So  $\theta_Y$  controls the distribution of  $Y$ , and  $\theta_X$  controls the conditional distribution of  $X$  given  $Y$ . The marginal distribution of  $X$  is then  $X \sim \mathcal{N}(0, \theta_Y + \theta_X)$ , which is what we can observe in the target domain. Clearly, from  $P(X)$  in the target domain,  $P(Y)$  or  $P(X|Y)$  is not identifiable because  $P(X)$  gives only  $\theta_Y + \theta_X$ . Now suppose we have prior distributions for  $\theta_Y$  and  $\theta_X$ :  $\theta_Y \sim \Gamma(3, 1)$  and  $\theta_X \sim \Gamma(1.5, 1)$ , where the two arguments are the shape and scale parameters of the gamma distribution, respectively. Figure 5(a) shows their prior distributions, and (b) gives the corresponding posterior distribution of  $\theta_Y$  given the

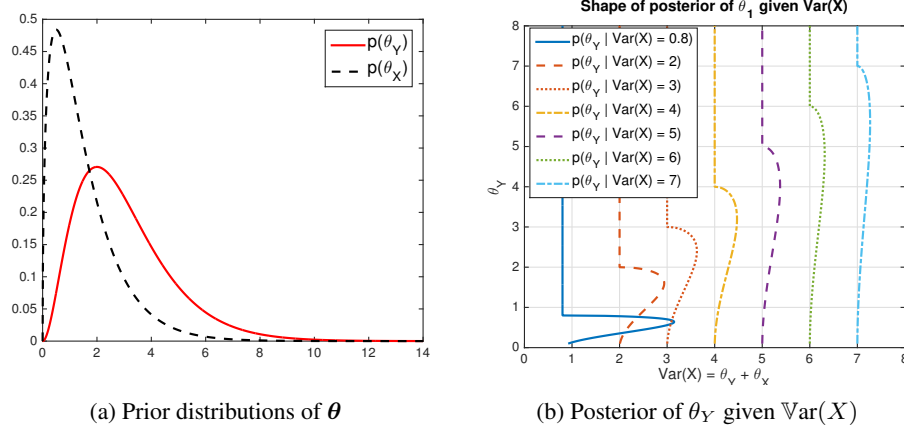


Figure 5: An illustration of the benefit of Bayesian treatment of the changeability of distribution modules (represented by the  $\theta$  variables).

variance of  $X$ , whose empirical version is observed in the target domain. One can see that although  $\theta_Y$  as well as  $\theta_X$  is not theoretically identifiable,  $P(\theta_Y | \text{Var}(X))$  is informative as to the value that  $\theta_Y$  may take. Especially when  $\text{Var}(X)$  is relatively small, the posterior distribution is narrow. The information we have about  $\theta_Y$  and  $X$  then allows non-trivial prediction of the target-domain joint distribution and the  $Y$  values from the values of  $X$ .

### A3. The Procedure of Learning the Augmented DAG

Denote by  $\mathbf{S}$  the set of  $Y$  and all  $X_i$ . The adapted DAG learning method has the following three steps.

**Step 1 (Finding changing distribution factors and estimating undirected graph)** Let  $C$  be the domain index. Apply the first stage of the PC algorithm to  $\mathbf{S} \cup \{C\}$  (the domain index  $C$  is added to the variable set to capture the changeability of the conditional distributions); it starts with an undirected, fully connected graph, removes the edge between two variables that are conditionally independent given some other variables, and finally determines the skeleton. It is interesting to note that if variable  $S_i \in \mathbf{S}$  is adjacent to  $C$ , then  $S_i$  is conditionally dependent on  $C$  given *any* subset of the remaining variables, and hence, there exists two different values of  $C$ ,  $c_1$  and  $c_2$ , such that  $P(S_i | \mathbb{P}\mathbf{A}(S_i), C = c_1) \neq P(S_i | \mathbb{P}\mathbf{A}(S_i), C = c_2)$ , meaning that  $P(S_i | \mathbb{P}\mathbf{A}(S_i))$  must change across domains. Also add variable  $\theta_{S_i}$  in the graph, which points to  $S_i$ .

**Step 2 (Determining edge direction with additional constraints)** We then find v-structures in the graph and do orientation propagation, as in the PC algorithm [38], but we benefit from additional constraints implied by the augmented DAG structure. In this procedure, we first make use of the constraint that if variable  $S_i$  is adjacent to  $C$ , then there exists a  $\theta$  variable,  $\theta_{S_i}$ , pointing to  $S_i$ ; given this direction, one may further determine the directions of other edges [36]. In particular, suppose  $S_j$  is adjacent to  $S_i$  but not to  $C$ . Then if it is conditionally independent from  $C$  given a variable set that does not include  $S_i$ , orient the edge between them as  $S_j \rightarrow S_i$ ; if it is conditionally independent from  $C$  given a variable set that includes  $S_i$ , orient it as  $S_j \leftarrow S_i$ . Second, if  $S_i$  and  $S_j$  are adjacent and are both adjacent to  $C$ , use the direction between them which gives independent changes in their conditional distributions,  $P(S_i | \mathbb{P}\mathbf{A}(S_i))$  and  $P(S_j | \mathbb{P}\mathbf{A}(S_j))$  [37]. If the changes are dependent in both directions, merge  $S_i$  and  $S_j$  as (part of) a “supernode” in the graph, and merge their corresponding  $\theta$  variables.

**Step 3 (Instantiating a DAG)** Step 2 produces a partially directed acyclic graph (PDAG), representing an Markov equivalence class [49]. All augmented DAGs in this equivalence class have the same (conditional) independence relations, so finally, we instantiate from the equivalence class a DAG over  $Y$  and the variables in its Markov Blanket (MB). (It was shown in Section 2 that inferring

the posterior of  $Y$  involves only the conditional distributions of  $Y$  and its children, not necessarily the conditional distribution of every feature.)

Two remarks are worth making on this procedure. First, to avoid strong assumptions on the forms of the conditional distributions, we make use of a nonparametric test of conditional independence, namely, kernel-based conditional independence test [50], when learning the augmented DAG. Second, given that the final inference for  $Y$  in the target domain depends only on the conditional distributions of  $Y$  and its children, one may extend some form of local graph structure discovery procedure (see, e.g., [51, 52]), to directly find the local graph structure involving  $Y$  and variables in its MB. This will be particularly beneficial on the computational load if we deal with high-dimensional features.

#### A4. Stochastic Variational Inference for Latent-Variable Conditional GAN

For better illustration of the inference procedure, we consider the situation where we do not use the graphical relations between  $X_i$  and  $Y$ . In this case, the data in all domains can be modeled by a specific LV-CGAN  $(X, Y) = g(E, \theta)$  with no condition variables. Once we have knowledge about the graphical model, either from domain prior or by learning, we can breakdown the generator into a series of LV-CGANs according to the graph. The details will be given in the next section. For now, we consider the learning and inference in a general generative model.

The log-likelihood terms in Eq. (5) can be considered as empirical estimation of the Kullback–Leibler (KL) divergence between the data distribution and model distribution. Specifically, the KL divergence between joint distribution of  $X$  and  $Y$  in the  $i$ th source domain and the model distribution  $p_g(X, Y|\theta)$  implied by the GAN generator  $g$  (with  $\theta$  as an input) can be calculated by

$$\begin{aligned} \text{KL}(P^{(i)}(X, Y)||p_g(X, Y|\theta)) \\ &= \int P^{(i)}(\mathbf{x}, y) \log P^{(i)}(\mathbf{x}, y) d\mathbf{x}dy - \int P^{(i)}(\mathbf{x}, y) \log p_g(\mathbf{x}, y|\theta) d\mathbf{x}dy \\ &= c_i - \int P^{(i)}(\mathbf{x}, y) \log p_g(\mathbf{x}, y|\theta) d\mathbf{x}dy, \end{aligned} \quad (\text{A1})$$

where the term  $c_i$  is considered as a constant because it does not contain any model parameters in  $g$ . The empirical estimation of  $\text{KL}(P^{(i)}(X, Y)||p_g(X, Y|\theta))$  is

$$\widehat{\text{KL}}(P^{(i)}(X, Y)||p_g(X, Y|\theta)) = \hat{c}_i - \frac{1}{m_i} \sum_{k=1}^{m_i} \log p_g(\mathbf{x}_k^{(i)}, y_k^{(i)}|\theta), \quad (\text{A2})$$

where  $\hat{c}_i$  is an empirical estimation of  $c_i$ . Similarly, we have the KL divergence between the marginal distribution of  $X$  in the target domain and the marginal distribution of  $X$  induced by the GAN generator  $g$ :

$$\widehat{\text{KL}}(P^\tau(X)||p_g(X|\theta)) = \hat{c}_\tau - \frac{1}{m} \sum_{k=1}^m \log p_g(\mathbf{x}_k^\tau|\theta). \quad (\text{A3})$$

For simplicity of notations, we assume all the source domains are of the same sample size, *i.e.*,  $m_1 = m_2 = \dots = m_s = m$ . If the sample sizes of the domains are different, we can apply biased batch sampling, which samples the same number of data points from each domain in a mini-batch. By multiplying both sides of Eq (5) by  $\frac{1}{m}$  and adding the constants  $-\hat{c}_i$  and  $-\hat{c}_\tau$ , we have

$$\begin{aligned} \frac{1}{m} \log p(\mathcal{D}) - \sum_{i=1}^s \hat{c}_i - \hat{c}_\tau &\geq -\frac{1}{m} \sum_{i=1}^s \text{KL}(q(\theta|\mathcal{D}^i)||p(\theta)) - \mathbb{E}_{q(\theta|\mathcal{D}^i)} \left[ \widehat{\text{KL}}(P^{(i)}(X, Y)||p_g(X, Y|\theta)) \right] \\ &\quad - \frac{1}{m} \text{KL}(q(\theta|\mathcal{D}^\tau)||p(\theta)) - \mathbb{E}_{q(\theta|\mathcal{D}^\tau)} \left[ \widehat{\text{KL}}(P^\tau(X)||p_g(X|\theta)) \right]. \end{aligned} \quad (\text{A4})$$

Since  $p_g(X, Y|\theta)$  and  $p_g(X|\theta)$  are implied by a GAN generator  $g$ , we cannot compute the  $\widehat{\text{KL}}$  terms in Eq. (A4). Instead, we replace the KL divergence with Maximum Mean Discrepancy (MMD) or Jensen-Shannon Divergence (JSD) that can compare the distributions of real data and the fake data generated from  $g$ . Specifically, given data  $(\mathbf{x}_k^{(i)}, y_k^{(i)})_{k=1}^B$  from the  $i$ th source domain, and data

$(\hat{\mathbf{x}}_k^{(i)}, \hat{y}_k^{(i)})_{k=1}^B$  from  $g(\cdot, \theta)$  (where  $B$  is the batch size), we have the following objective:

$$\begin{aligned} \max_{g, q} & -\frac{1}{m} \sum_{i=1}^s \text{KL}(q(\theta|\mathcal{D}^i)|p(\theta)) - \mathbb{E}_{q(\theta|\mathcal{D}^i)} \left[ \widehat{\text{Div}}(P^{(i)}(X, Y)||p_g(X, Y|\theta)) \right] \\ & -\frac{1}{m} \text{KL}(q(\theta|\mathcal{D}^\tau)|p(\theta)) - \mathbb{E}_{q(\theta|\mathcal{D}^\tau)} \left[ \widehat{\text{Div}}(P^\tau(X)||p_g(X|\theta)) \right], \end{aligned} \quad (\text{A5})$$

where  $\text{Div}$  can be MMD, JSD or any other divergence measures that can measure the distance between the real and fake samples. The empirical MMD between real and fake data is defined as

$$\begin{aligned} \widehat{\text{MMD}}(P^{(i)}(X, Y)||p_g(X, Y|\theta)) &= \frac{1}{B^2} \sum_{k=1}^B \sum_{k'=1}^B k(\mathbf{x}_k^{(i)}, \mathbf{x}_{k'}^{(i)}) l(y_k^{(i)}, y_{k'}^{(i)}) - \\ & \frac{2}{B^2} \sum_{k=1}^B \sum_{k'=1}^B k(\mathbf{x}_k^{(i)}, \hat{\mathbf{x}}_{k'}^{(i)}) l(y_k^{(i)}, \hat{y}_{k'}^{(i)}) + \frac{1}{B^2} \sum_{k=1}^B \sum_{k'=1}^B k(\hat{\mathbf{x}}_k^{(i)}, \hat{\mathbf{x}}_{k'}^{(i)}) l(\hat{y}_k^{(i)}, \hat{y}_{k'}^{(i)}), \end{aligned}$$

where  $k$  and  $l$  are kernel functions for  $\mathbf{x}$  and  $y$ , respectively. The target-domain empirical MMD is of the same form except that  $l$  function needs to be removed because only marginal distributions of  $X$  are compared. According to the GAN formulation [39, 40], Jensen-Shannon Divergence (JSD) can be implemented by introducing a discriminator  $D$ :

$$\widehat{\text{JSD}}(P^{(i)}(X, Y)||p_g(X, Y|\theta)) = \max_D \frac{1}{B} \sum_{k=1}^B [\log D(\mathbf{x}_k, y_k)] + \frac{1}{B} \sum_{k=1}^B [\log(1 - D(\hat{\mathbf{x}}_k, \hat{y}_k))].$$

The target-domain JSD can be obtained by omitting  $y_k$  and  $\hat{y}_k$  in the formulation.

Finally, we can make use of Eq. A5 to learn the posterior distribution  $q$  and generator  $g$  in an end-to-end manner. For the expectation  $\mathbb{E}_{q(\theta|\mathcal{D}^i)}[\cdot]$ , we use the reparameterization trick [53] and sample  $\theta_j^{(i)}$  from the model  $\theta = \mu^{(i)} + \epsilon * \sigma^{(i)}$ , where  $\epsilon$  is a standard normal variable, such that the variational parameters in the posterior distribution of  $\theta$  can be simultaneously learned with  $g$ . If assuming the prior  $p(\theta) = \mathcal{N}(0, \mathbf{I})$ , the KL divergence terms  $\text{KL}(q(\theta|\mathcal{D}^{(i)})|p(\theta))$  have the following closed form solution:

$$\text{KL}(q(\theta|\mathcal{D}^{(i)})|p(\theta)) = \frac{1}{2} \sum_{j=1}^d (-1 - \log((\sigma_j^{(i)})^2) + (\mu_j^{(i)})^2 + (\sigma_j^{(i)})^2), \quad (\text{A6})$$

where  $d$  is the dimensionality of  $\theta$ .  $\text{KL}(q(\theta|\mathcal{D}^\tau)|p(\theta))$  can be calculated in the same way.

## A5. Factorized Inference and Learning According to the Augmented DAG

In the previous section, we have shown the approximate inference and learning procedure when not taking into consideration of graph structure. In this section, we will show how the inference and learning procedure can be simplified given an augmented DAG. According to Eq. 4, we only need to consider the set  $\mathbf{V} = \mathbb{CH}(Y) \cup \{Y\}$  for prediction of  $Y$  in the target domain. According to an augmented DAG, we have the following factorization  $P(\mathbf{V}|\theta) = \prod_{V_j \in \mathbf{V}} P(V_j | \mathbb{PA}(V_j), \theta_{V_j})$ . According to the factorization, we can calculate the posterior of  $\theta$  in the  $i$ th source domain as

$$\begin{aligned} P(\theta|\mathcal{D}^i) &= \frac{\prod_k \prod_{V_j \in \mathbf{V}} P(v_{jk}^{(i)} | \mathbb{PA}(v_{jk}^{(i)}), \theta_{V_j}) P(\theta_{V_j})}{\int \prod_k \prod_{V_j \in \mathbf{V}} P(v_{jk}^{(i)} | \mathbb{PA}(v_{jk}^{(i)}), \theta_{V_j}) P(\theta_{V_j}) d\theta_{V_j}} \\ &= \frac{\prod_{V_j \in \mathbf{V}} \prod_k P(v_{jk}^{(i)} | \mathbb{PA}(v_{jk}^{(i)}), \theta_{V_j}) P(\theta_{V_j})}{\prod_{V_j \in \mathbf{V}} \prod_k \int P(v_{jk}^{(i)} | \mathbb{PA}(v_{jk}^{(i)}), \theta_{V_j}) P(\theta_{V_j}) d\theta_{V_j}} \\ &= \prod_{V_j \in \mathbf{V}} P(\theta_{V_j}|\mathcal{D}^i). \end{aligned} \quad (\text{A7})$$

However, the target domain  $\theta$  posterior cannot be factorized in this way because the marginalization w.r.t.  $y_k^\tau$ , as shown in Eq. 4. Therefore, we can simplify the inference and learning procedure (A5) by

making use of the factorization in the source domain as

$$\begin{aligned} \max_{g,q} - \frac{1}{m} \sum_{i=1}^s \sum_{j=1}^{|V|} \text{KL}(q(\theta_{V_j} | \mathcal{D}^i) | p(\theta_{V_j})) - \mathbb{E}_{q(\theta_{V_j} | \mathcal{D}^i)} \left[ \widehat{\text{Div}}(P^{(i)}(V_j, \mathbb{P}\mathbb{A}(V_j)) | p_{g_j}(V_j, \mathbb{P}\mathbb{A}(V_j) | \theta_{V_j})) \right] \\ - \frac{1}{m} \text{KL}(q(\boldsymbol{\theta} | \mathcal{D}^\tau) | p(\boldsymbol{\theta})) - \mathbb{E}_{q(\boldsymbol{\theta} | \mathcal{D}^\tau)} \left[ \widehat{\text{Div}}(P^\tau(X) | p_g(X | \boldsymbol{\theta})) \right], \end{aligned} \quad (\text{A8})$$

where  $p_{g_j}(V_j, \mathbb{P}\mathbb{A}(V_j) | \theta_{V_j})$  is the distribution specified by the LV-CGAN  $V_j = g_j(E_j, \mathbb{P}\mathbb{A}(V_j), \theta_{V_j})$  and  $p_g(X | \boldsymbol{\theta})$  is the marginal distribution of  $X$  specified by a composition of all the LV-CGANs  $g_j$  according to the augmented DAG.

After obtaining the approximate posterior distribution  $q(\boldsymbol{\theta} | \mathcal{D}^\tau)$  and the LV-CGAN generator, we can perform prediction in the target domain by approximating Eq. 4 as

$$\begin{aligned} P(y_k^\tau | \mathbf{x}^\tau) &= \int P(y_k^\tau | \mathbf{x}_k^\tau, \boldsymbol{\theta}) q(\boldsymbol{\theta} | \mathcal{D}^\tau) d\boldsymbol{\theta} \\ &\approx \frac{1}{L} \sum_{l=1}^L P(y_k^\tau | \mathbf{x}_k^\tau, \theta_l), \end{aligned} \quad (\text{A9})$$

where  $\theta_l \sim q(\boldsymbol{\theta} | \mathcal{D}^\tau)$  and  $P(y_k^\tau | \mathbf{x}_k^\tau, \theta_l)$  is estimated by training a softmax classifier on the data generated from the LV-CGAN generator with  $\theta_l$  as inputs.

## A6. Learned Graph on WiFi Dataset

Figure 6 shows the learned augmented DAG on the WiFi localization dataset (t1 & t2). The graphs learned on t2 & t3 and t1 & t3 are almost identical to the graph shown in Figure 6.

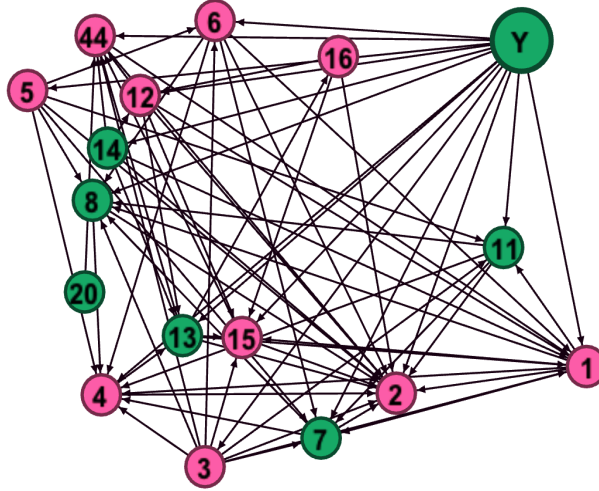


Figure 6: The augmented DAG learned on the WiFi t1 and t2 datasets. Pink nodes denote the changing modules and green ones denote the constant modules whose conditional distribution does not change across domains.

## A7. Implementation Details in Digit Adaptation Experiments

To generate high-quality images, we build our model based on BigGAN [54]. We choose a simple architecture and the generator and discriminator used are shown in Table 4.

For convenience, we use the following abbreviation: C = Feature channel, K = Kernel size, S = Stride size, SNLinear = A linear layer with spectral normalization (SN), and SNResBlk = A residual block with SN. The dimensionality of input noise  $E$  is 128.

Because the original CGAN formulation [40] that feeds the concatenation of the label and image into a discriminator  $D$  usually cannot generate high-quality images, we utilize the recent Twin Auxiliary Classifier GAN (TAC-GAN) framework [48] to match conditional distributions of generated and real data in the source domains. Specifically, the formulation contains the following modules after the shared feature extraction residual blocks: 1) the discriminator SNLinear (D) to distinguish real and generated images, 2) the primary auxiliary classifier (AC) to predict class labels of real images in source domains, 3) the twin auxiliary classifier (TAC) to predict labels of all generated images from CGAN generator, 4) the primary domain classifier (DC) to predict domain labels of all data, and 5) the twin domain classifier (TDC) to predict domain labels of all generated images from the CGAN generator.

Table 4: Network architecture for digits adaptation.

Generator				
Index	Layer	C	K	S
1	SNLinear	256*4		
2	Upsample SNResblk	256	3	1
3	Upsample SNResblk	256	3	1
4	Upsample SNResblk	256	3	1
5	Relu+SNConv+Tanh	3	3	1
Discriminator				
1	Downsample SNResblk	256	3	1
2	Downsample SNResblk	256	3	1
3	Downsample SNResblk	256	3	1
4	AveragePooling	256		
5 <sub>1</sub>	SNLinear (D)	1		
5 <sub>2</sub>	SNLinear (AC)	10		
5 <sub>3</sub>	SNLinear (TAC)	10		
5 <sub>4</sub>	SNLinear (DC)	4		
5 <sub>5</sub>	SNLinear (TDC)	4		

## A8. The Generated Images in Digit Adaptation Experiments

Figure 7 and Figure 8 show the generated images in the S+M+D/T and M+T+D/S tasks, respectively. The last image is the generated image from LV-CGAN conditioned on the labels. Though the target domain is unlabeled, our method successfully transfers information from the labeled source domains and reconstruct the conditional distributions  $P(X|Y)$  in the target domain.

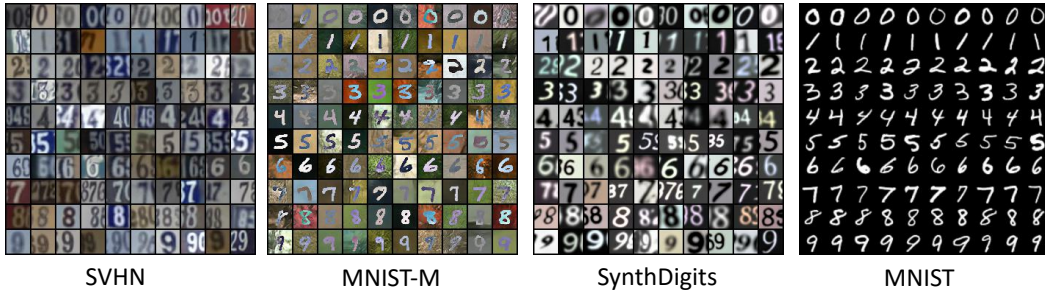


Figure 7: The generated images in each domain in the S+M+D/T task. Each row of an image corresponds to a fixed  $Y$  value, ranging from 0 to 9. MNIST is the unlabeled target domain and the rest are source domains.

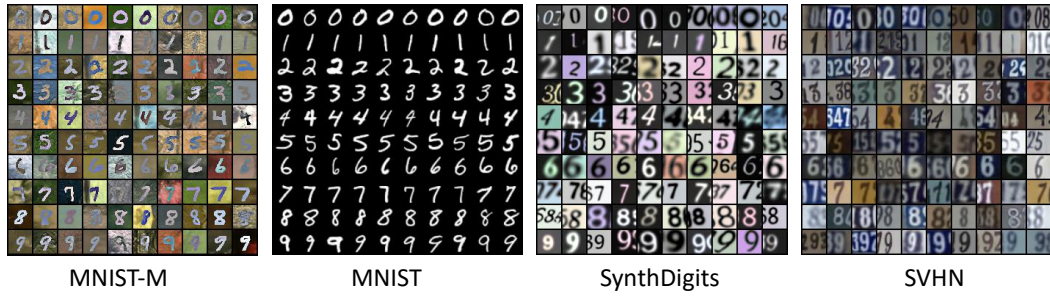


Figure 8: The generated images in each domain in the M+T+D/S task. Each row of an image corresponds to a fixed  $Y$  value, ranging from 0 to 9. SVHN is the unlabeled target domain and the rest are source domains.



## References

- [1] H. Shimodaira. Improving predictive inference under covariate shift by weighting the log-likelihood function. *Journal of Statistical Planning and Inference*, 90:227–244, 2000.
- [2] B. Zadrozny. Learning and evaluating classifiers under sample selection bias. In *ICML-04*, pages 114–121, Banff, Canada, 2004.
- [3] J. Huang, A. Smola, A. Gretton, K. Borgwardt, and B. Schölkopf. Correcting sample selection bias by unlabeled data. In *NIPS 19*, pages 601–608, 2007.
- [4] M. Sugiyama, T. Suzuki, S. Nakajima, H. Kashima, P. von Büna, and M. Kawanabe. Direct importance estimation for covariate shift adaptation. *Annals of the Institute of Statistical Mathematics*, 60:699–746, 2008.
- [5] S. Ben-David, S. Shalev-Shwartz, and Ruth Uner. Domain adaptation—can quantity compensate for quality? In *ISAIM 2012*, 2012.
- [6] C. Cortes, Y. Mansour, and M. Mohri. Learning bounds for importance weighting. In *NIPS 23*, 2010.
- [7] S. J. Pan, I. W. Tsang, J. T. Kwok, and Q. Yang. Domain adaptation via transfer component analysis. *IEEE Transactions on Neural Networks*, 22:199–120, 2011.
- [8] M. Baktashmotlagh, M.T. Harandi, B.C. Lovell, and M. Salzmann. Unsupervised domain adaptation by domain invariant projection. In *ICCV 2013*, pages 769–776, Dec 2013.
- [9] B. Gong, K. Grauman, and F. Sha. Connecting the dots with landmarks: Discriminatively learning domain-invariant features for unsupervised domain adaptation. In *ICML*, pages 222–230, 2013.
- [10] M. Long, Y. Cao, J. Wang, and M. Jordan. Learning transferable features with deep adaptation networks. In *ICML-15*, pages 97–105, 2015.
- [11] Y. Ganin, E. Ustinova, H. Ajakan, P. Germain, H. Larochelle, F. Laviolette, M. Marchand, and V. Lempitsky. Domain-adversarial training of neural networks. *Journal of Machine Learning Research*, 17(1):2096–2030, 2016.
- [12] A. Storkey. When training and test sets are different: Characterizing learning transfer. In J. Candela, M. Sugiyama, A. Schwaighofer, and N. Lawrence, editors, *Dataset Shift in Machine Learning*, pages 3–28. MIT Press, 2009.
- [13] B. Schölkopf, D. Janzing, J. Peters, E. Sgouritsa, K. Zhang, and J. Mooij. On causal and anticausal learning. In *ICML-12*, Edinburgh, Scotland, 2012.
- [14] K. Zhang, B. Schölkopf, K. Muandet, and Z. Wang. Domain adaptation under target and conditional shift. In *ICML-13*, 2013.
- [15] K. Zhang, M. Gong, and B. Schölkopf. Multi-source domain adaptation: A causal view. In *Twenty-Ninth AAAI Conference on Artificial Intelligence*, 2015.
- [16] M. D. Plessis and M. Sugiyama. Semi-supervised learning of class balance under class-prior change by distribution matching. In *ICML-12*, pages 823–830, 2012.
- [17] A. Iyer, A. Nath, and S. Sarawagi. Maximum mean discrepancy for class ratio estimation: Convergence bounds and kernel selection. In *Proc. ICML 2014*, 2014.
- [18] Z. C. Lipton, Y. Wang, and A. Smola. Detecting and correcting for label shift with black box predictors. *arXiv preprint arXiv:1802.03916*, 2018.
- [19] T. Liu D. Tao C. Glymour M. Gong, K. Zhang and B. Schölkopf. Domain adaptation with conditional transferable components. In *ICML 2016*, 2016.
- [20] M. Long, J. Wang, G. Ding, J. Sun, and P. S. Yu. Transfer feature learning with joint distribution adaptation. In *Proceedings of the IEEE international conference on computer vision*, pages 2200–2207, 2013.
- [21] Q. Chen, Y. Liu, Z. Wang, I. Wassell, and K. Chetty. Re-weighted adversarial adaptation network for unsupervised domain adaptation. In *Proceedings of the IEEE Conference on Computer Vision and Pattern Recognition*, pages 7976–7985, 2018.
- [22] M. Long, H. Zhu, J. Wang, and M. I. Jordan. Deep transfer learning with joint adaptation networks. In *Proc. 34th International Conference on Machine Learning (ICML 2017)*, 2017.
- [23] N. Courty, R. Flamary, A. Habrard, and A. Rakotomamonjy. Joint distribution optimal transportation for domain adaptation. In *NIPS*, 2017.
- [24] J. Pearl. *Probabilistic Reasoning in Intelligent Systems: Networks of Plausible Inference*. Morgan Kaufmann, 1988.
- [25] D. Koller and N. Friedman. *Probabilistic Graphical Models: Principles and Techniques*. MIT Press, Cambridge, MA, 2009.
- [26] Y. Mansour, M. Mohri, and A. Rostamizadeh. Domain adaptation with multiple sources. In *NIPS 19*, pages 1041–1048, Cambridge, MA, 2008. MIT Press.

- [27] J. Gao, W. Fan, J. Jiang, and J. Han. Knowledge transfer via multiple model local structure mapping. In *International Conference on Knowledge Discovery and Data Mining, Las Vegas, NV*, 2008.
- [28] L. Duan, I. W. Tsang, D. Xu, and T. S. Chua. Domain adaptation from multiple sources via auxiliary classifiers. In *ICML*, 2009.
- [29] R. Chattopadhyay, J. Ye, S. Panchanathan, W. Fan, and I. Davidson. Multi-source domain adaptation and its application to early detection of fatigue. In *KDD*, 2011.
- [30] Judea Pearl. A probabilistic calculus of actions. In *UAI 1994*, pages 454–462, 1994.
- [31] E. Pearl and E. Bareinboim. Transportability of causal and statistical relations: A formal approach. In *AAAI 2011*, pages 247–254, 2011.
- [32] S. Magliacane, T. van Ommen, T. T. Claassen, S. Bongers, P. Versteeg, and J. M. Mooij. Domain adaptation by using causal inference to predict invariant conditional distributions. In *NIPS*, 2018.
- [33] E. Bareinboim, J. Tian, and J. Pearl. Recovering from selection bias in causal and statistical inference. In *Proc. 28th AAAI Conference on Artificial Intelligence*, pages 2410–2416, 2014.
- [34] P. Spirtes, C. Glymour, and R. Scheines. *Causation, Prediction, and Search*. Springer-Verlag Lectures in Statistics, 1993.
- [35] M. Gong, K. Zhang, T. Liu, D. Tao, C. Glymour, and B. Schölkopf. Domain adaptation with conditional transferable components. In *Proceedings of the 33rd International Conference on Machine Learning (ICML 2016)*, volume 48, pages 2839–2848, 2016.
- [36] K. Zhang, B. Huang, J. Zhang, C. Glymour, and B. Schölkopf. Causal discovery from nonstationary/heterogeneous data: Skeleton estimation and orientation determination. In *IJCAI*, volume 2017, page 1347, 2017.
- [37] B. Huang, K. Zhang, J. Zhang, R. Sanchez Romero, C. Glymour, and B. Schölkopf. Behind distribution shift: Mining driving forces of changes and causal arrows. In *ICDM 2017*, 2017.
- [38] P. Spirtes, C. Glymour, and R. Scheines. *Causation, Prediction, and Search*. MIT Press, Cambridge, MA, 2nd edition, 2001.
- [39] Ian Goodfellow, Jean Pouget-Abadie, Mehdi Mirza, Bing Xu, David Warde-Farley, Sherjil Ozair, Aaron Courville, and Yoshua Bengio. Generative adversarial nets. In *Advances in neural information processing systems*, pages 2672–2680, 2014.
- [40] Mehdi Mirza and Simon Osindero. Conditional generative adversarial nets. *arXiv preprint arXiv:1411.1784*, 2014.
- [41] Matthew D Hoffman, David M Blei, Chong Wang, and John Paisley. Stochastic variational inference. *The Journal of Machine Learning Research*, 14(1):1303–1347, 2013.
- [42] A. Gretton, K. Fukumizu, Z. Harchaoui, and B. K. Sriperumbudur. A fast, consistent kernel two-sample test. In *NIPS 23*, pages 673–681, Cambridge, MA, 2009. MIT Press.
- [43] K. Muandet, D. Balduzzi, and B. Schölkopf. Domain generalization via invariant feature representation. In *Proceedings of the 30th International Conference on Machine Learning, JMLR: W&CP Vol. 28*, 2013.
- [44] G. Blanchard, G. Lee, and C. Scott. Generalizing from several related classification tasks to a new unlabeled sample. In *NIPS 2011*, pages 2178–2186, 2011.
- [45] Kai Zhang, V. Zheng, Q. Wang, J. Kwok, Q. Yang, and I. Marsic. Covariate shift in hilbert space: A solution via surrogate kernels. In *Proceedings of the 30th International Conference on Machine Learning*, pages 388–395, 2013.
- [46] Han Zhao, Shanghang Zhang, Guanhang Wu, José MF Moura, Joao P Costeira, and Geoffrey J Gordon. Adversarial multiple source domain adaptation. In *Advances in neural information processing systems*, pages 8559–8570, 2018.
- [47] Ryan Remy Brinkman, Maura Gasparetto, Shang-Jung Jessica Lee, Albert J Ribickas, Janelle Perkins, William Janssen, Renee Smiley, and Clay Smith. High-content flow cytometry and temporal data analysis for defining a cellular signature of graft-versus-host disease. *Biology of Blood and Marrow Transplantation*, 13(6):691–700, 2007.
- [48] Mingming Gong, Yanwu Xu, Chunyuan Li, Kun Zhang, and Kayhan Batmanghelich. Twin auxiliary classifiers gan. In *Advances in Neural Information Processing Systems*, pages 1328–1337, 2019.
- [49] T. Verma and J. Pearl. Equivalence and synthesis of causal models. In *UAI 1990*, pages 255–270, 1991.
- [50] K. Zhang, J. Peters, D. Janzing, and B. Schölkopf. Kernel-based conditional independence test and application in causal discovery. In *UAI 2011*, 2011.
- [51] G. F. Cooper. A simple constraint-based algorithm for efficiently mining observational databases for causal relationships. *Data Mining and Knowledge Discovery*, 1:203–224, 1997.
- [52] T. Gao and Q. Ji. Local causal discovery of direct causes and effects. In *NIPS’15*, pages 2503–2511, 2015.
- [53] Diederik P Kingma and Max Welling. Auto-encoding variational bayes. *arXiv preprint arXiv:1312.6114*, 2013.

- [54] Andrew Brock, Jeff Donahue, and Karen Simonyan. Large scale gan training for high fidelity natural image synthesis. *arXiv preprint arXiv:1809.11096*, 2018.